



MCM-41 supported PdNi catalysts for dry reforming of methane

S. Damyanova^{a,*}, B. Pawelec^b, K. Arishtirova^a, J.L.G. Fierro^b, C. Sener^c, T. Dogu^c

^a Institute of Catalysis, Bulgarian Academy of Sciences, 1113 Sofia, Bulgaria

^b Instituto de Catálisis y Petroleoquímica, CSIC, Cantoblanco, 28049 Madrid, Spain

^c Department of Chemical Engineering, Middle East Technical University, 06531 Ankara, Turkey

ARTICLE INFO

Article history:

Received 9 March 2009

Received in revised form 21 July 2009

Accepted 23 July 2009

Available online 8 August 2009

Keywords:

Dry CH₄ reforming

Bimetallic PdNi catalysts

Coke

Characterization

ABSTRACT

A series of bimetallic PdNi catalysts supported on mesoporous MCM-41 with different Ni content (Ni/Si ratio of 0.2–0.4) was synthesized. The effect of Pd addition to Ni-containing catalysts as well as the effect of the Ni content on the surface and catalytic properties of the catalysts was studied. The samples were characterized using various techniques, such as energy-dispersive X-ray spectroscopy, N₂ adsorption–desorption isotherms, X-ray diffraction, thermogravimetric and differential analyses, X-ray photoelectron spectroscopy, high resolution transmission electron microscopy and temperature-programmed reduction. Reforming of methane with carbon dioxide was used as a test reaction. The results indicated that the addition of a small amount of Pd (0.5%) to Ni-containing catalysts leads to formation of small nano-sized, easy reducible NiO particles. Agglomeration of NiO as well as of metallic nickel phase over PdNi samples increased with increasing the Ni content. Formation of filamentous carbon over surface of spent monometallic Ni and bimetallic PdNi catalyst was observed. In spite of filamentous carbon deposition, the catalytic activity and stability of bimetallic PdNi catalysts are higher than those of monometallic Ni one. Within bimetallic system, the PdNi catalyst with Ni/Si ratio of 0.3 revealed the best performance and stability caused by presence of small nickel particles well dispersed on the catalyst surface.

© 2009 Elsevier B.V. All rights reserved.

1. Introduction

Carbon dioxide (dry) reforming of methane has received considerable attention as a promising way that enables the utilization of natural gas, reduction of greenhouse gases and hydrogen production. The dry reforming produces synthesis gas with an appropriate molar ratio for several applications as methanol synthesis, Fisher–Tropsch reaction and acetic acid synthesis [1]. However, the major difficulty in realization of methane reforming with CO₂ is the thermodynamically favoured coke formation, which deactivates the catalysts. Different catalysts have been developed for this reaction. A number of noble metals, such as Pt, Pd, Rh and Ru, have shown to be active in dry reforming by minimizing coke formation [2–5]. However, the low availability and high cost of noble metals make them unsuitable for industrial size operations. Nickel has emerged as a possible alternative due to its low cost. Nickel-based catalysts have shown high methane conversion and good product selectivity [6,7]. However, these catalysts deactivate quickly because of carbon deposition.

Strategies to prevent coke formation and to improve the lifetime of Ni-based catalysts include: (i) use of different promoters to modifying the acid–base and redox properties of the catalyst; (ii) enhancement of metal dispersion and decreasing particle size; (iii) optimization of physical and chemical properties of the catalyst supports; (iv) improvement of catalyst preparation methodology; and (v) addition of a small amount of noble metal to nickel catalyst, etc.

Considerable research has been conducted on the modification of catalyst supports using promoters to overcome the deactivation associated with nickel-based catalysts. It has been reported that the addition of K and Ca can significantly inhibit carbon formation due to the favourable adsorption of acidic CO₂ on the basic surface sites [8,9]. Silver [10] or magnesium [11] has been used as promoters modifying the properties of alumina by increasing the basicity and accelerating the CH₄ activation. Strong metal–support interactions have proven to reduce nickel sintering which can accelerate coke formation [12,13]. The plasma treated Ni/Al₂O₃ catalyst containing high concentration of close packed plane with improved Ni dispersion and enhanced Ni–alumina interaction has shown high catalytic activity in dry methane reforming and resistance to carbon formation [14]. Alumina–aluminum phosphate (AAP) materials [15] have been used as a support for Ni catalysts and it was shown that the method of deposition of the

* Corresponding author. Tel.: +359 29792588; fax: +359 29712967.

E-mail address: sonia.damyanova@yahoo.com (S. Damyanova).

active metal is very important for stable reforming catalyst. Average pore size of these materials was substantially reduced when nickel is impregnated on the support, whereas the large pores and high surface area are maintained when nickel is co-precipitated with AAP. Ni-Co bimetallic catalysts composed by co-precipitating Ni-, Co-, Al- and Mg-containing precursor solutions demonstrated excellent performance for dry methane reforming [16] coming from the synergetic effect, good metal dispersion and strong metal support interaction.

Other promising alternative to suppress or minimize the carbon formation is the use of small amount of noble metal as promoter for nickel catalysts. It was shown [17] that the highly dispersed Rh over Al_2O_3 exhibited high coke resistance ability and high reforming activity. The addition of noble metal such as Rh, Pt and Pd to NiO–MgO solid solution was also effective to the inhibition of carbon deposition [18]. The addition of Ru or Pd to Ni/SiO₂ strongly enhanced the activity and stability of the catalyst in the process of dry reforming [19]. Perovskite-type oxide $\text{LaNi}_{0.8}\text{Ru}_{0.2}\text{O}_3$ have been develop as promising catalyst for dry methane reforming due to its high resistant to coke formation [20]. Our recent results showed that the addition of a small amount of Pt to zeolite-supported Ni catalysts [21] improved their catalytic performance and coke resistance due to the “dilution” effect of Pt leading to high nickel dispersion.

The present work is a continuation of the previously our work [22] related to study the surface and catalytic properties of monometallic nickel catalysts with different Ni content. In this work, we attempted to develop effective nickel-containing catalysts modified with a small amount of Pd that result in bimetallic catalysts assuring both high activity and stability. MCM-41 was used as a carrier for supported Ni catalysts [22]. Mesoporous materials, which possess large pores, thick walls and high thermal stability have been used as a promising catalyst support, particularly for reactions occurring at high temperatures [23,24]. Controllable pore size in the mesopore regime is sought since the coke deposition is more susceptible in micropore channels. It was shown that Ni-Co catalysts supported on mesoporous silica material are active, selective and stable catalysts for dry reforming of methane [24]. The effect of both, the Pd addition and Ni content on the surface and catalytic properties of MCM-41-supported Ni was studied. The samples were characterized by energy-dispersive X-ray spectroscopy (EDS), N₂ adsorption–desorption isotherms, X-ray diffraction (XRD), thermogravimetric and differential thermal analyses (TG/DTA), X-ray photoelectron spectroscopy (XPS), high resolution transmission electron microscopy (HRTEM) and temperature-programmed reduction (TPR). The catalytic properties of the catalysts were evaluated in the reaction of reforming of methane with CO₂.

2. Experimental

2.1. Sample preparation

MCM-41 was prepared according to the following procedure. Hexadecyl trimethylammonium bromide ($\text{C}_{16}\text{H}_{33}(\text{CH}_3)_3\text{NBr}$ (CTMABr), Merck 99% pure) was used as surfactant and sodium silicate solution (27 wt% SiO₂, Aldrich) was the silicate source. 13.2 g CTMABr was dissolved in 87 ml deionised water. Clear solution was obtained by continuous stirring at a rate of 500 rpm while the solution temperature was kept at 303 K. 11.3 ml sodium silicate solution was added drop wise to the solution of surfactant. The pH of the mixture was adjusted to 11.0 by a solution of H₂SO₄. The resulting gel was stirred for 1 h. Final synthesis gel was transferred to a teflon bottle and placed in a stainless-steel autoclave. The hydrothermal synthesis was carried out at 393 K for 96 h. The resultant solid was recovered by filtration and washed

with deionised water. After washing, MCM-41 was dried at 313 K in vacuum for 24 h. MCM-41 was finally calcined by heating from ambient temperature to 823 K at a rate of 1 K/min and kept at 823 K for 6 h in a flow of dry air in a tubular furnace.

Bimetallic PdNi catalysts supported on MCM-41 were prepared by sequential impregnation using an aqueous precursor solutions of $\text{Ni}(\text{NO}_3)_2 \cdot 6\text{H}_2\text{O}$ (first step) and $\text{Pd}(\text{NO}_3)_2 \cdot 2\text{H}_2\text{O}$ (second step). The Ni-containing solids were dried at 383 K for 12 h in air atmosphere. After the Pd addition, all samples were dried at 383 K and calcined at 823 K in air atmosphere for 12 and 4 h, respectively. The amount of Pd was 0.5 wt%. The ratio of Ni/Si was in the range of 0.2–0.4. The samples were labelled as xPdNi where x is the ratio of Ni/Si.

2.2. Characterization

2.2.1. Chemical analysis

Metal loadings (Pd, Ni) of the samples were determined by energy-dispersive X-ray spectroscopy (EDS) analysis using a Jeol JSM-6400 apparatus. The Ni/Si ratio estimated from chemical compositions of the samples is presented in Table 1.

2.2.2. Nitrogen-adsorption isotherms

The textural properties of the calcined samples previously degassed at 573 K for 24 h were measured based on N₂ adsorption–desorption isotherms using a Micromeritics ASAP-2000 apparatus. The specific surface areas of the samples were determined using the nitrogen-adsorption data from the relative equilibrium pressure interval of 0.03–0.3 P/P^0 according to the standard BET procedure. Pore distribution was calculated from the desorption branch of the corresponding nitrogen isotherm employing the Barret–Joyner–Halenda (BJH) method.

2.2.3. X-ray powder diffraction

X-ray diffraction profiles were recorded on a computerized Seifert 3000XRD diffractometer using Cu K α ($\lambda = 0.15406$ nm) radiation and a PW 2200 Bragg–Brentano $\theta/2\theta$ goniometer equipped with a bent graphite monochromator and an automatic slit. Diffraction peaks were recorded in a 2θ range between 10° and 90°. Step size of 0.03° and step scan of 10.0 s have been used to identify the structure of the samples. The apparent crystallite size was determined using the Scherrer equation [25].

2.2.4. X-ray photoelectron spectroscopy

Photoelectron spectra of freshly H₂-reduced (*in situ* at 773 K) catalysts were recorded on a VG Escalab 200R electron spectrometer equipped with a hemispherical electron analyzer, using a Mg K α ($h\nu = 1253.6$ eV, $1 \text{ eV} = 1.603 \times 10^{-19}$ J) X-ray source. After degassing at 10^{-6} mbar, the samples were transferred to the ion-pumped analysis chamber, in which residual pressure was kept below 4×10^{-9} mbar during data acquisition. The binding energies (BE) of Si 2p, O 1s, Pd 3d_{5/2} and Ni 2p_{3/2} core-levels were recorded. The binding energy of the C 1s peak at 284.9 eV was taken as an internal standard. The accuracy of the BE values was ± 0.1 eV. The

Table 1

Textural properties of MCM-41 supported monometallic Ni and bimetallic PdNi catalysts.

Sample	Ni/Si	S_{BET} (m ² /g)	Pore volume (cm ³ /g)	Pore diameter (nm)	D_{XRD} NiO (nm)	D_{XRD} PdO (nm)
MCM-41	–	1358	1.250	2.701	–	–
0.3Ni	0.3	580.7	0.391	2.185	25.7	–
0.2PdNi	0.2	523.6	0.383	2.392	13.9	5.8
0.3PdNi	0.3	514.7	0.352	2.239	12.3	6.4
0.4PdNi	0.4	506.6	0.348	2.108	20.5	6.8

invariance of the peak shapes and widths at the beginning and at the end of the analyses indicated absence of differential charging. The peaks were fitted by a non-linear least square fitting routine using a properly weighted sum of Lorentzian and Gaussian component curves after background subtraction according to Shirley [26] and Sherwood [27]. Surface atomic concentration was evaluated from peak areas using appropriate sensitivity factors built in the VG instrument software.

2.2.5. Temperature-programmed reduction

The temperature-programmed reduction studies were performed in a semiautomatic Micromeritics TPD/TPR 2900 apparatus interfaced with a computer. The sample of 0.050 g was housed in a quartz tubular reactor and TPR profiles were obtained by passing a 10% H₂/Ar flow (60 ml/min) through the sample. Temperature was increased at a rate of 15 K/min from room temperature to 1000 K and the amount of H₂ consumed was determined with a thermal conductivity detector. A cooling trap placed between the sample and the detector retained the water formed during the reduction process.

2.2.6. High resolution transmission electron microscopy

HRTEM studies were carried out using a JEM 2100F microscope operating with a 200 kV accelerating voltage and fitted with an INCA X-sight (Oxford Instruments) energy-dispersive X-ray microanalysis (EDX) system to verify semi-quantitative composition of supported phases. The pre-reduced (5% H₂/He, 773 K, 1 h) and spent catalysts were ground into a fine powder and dispersed ultrasonically in hexane at room temperature. Then, a drop of the suspension was put on a lacey carbon-coated Cu grid. At least 10 representative images were taken for each sample. In order to obtain statistically reliable information, the size of ca. 200 particles was measured.

2.2.7. Thermogravimetric and differential thermal analyses

In order to quantify the coke deposits formed in the used catalyst during the reaction of CO₂ reforming of methane, the spent catalysts were subjected to temperature-programmed oxidation in a 20% O₂/N₂ mixture by raising the temperature from room temperature to 1073 K at a rate of 10 K/min. These experiments were conducted in a TGA/SDTA851 equipment (Mettler Toledo).

2.2.8. Activity measurements

The catalytic experiments in the reaction of reforming of CH₄ with CO₂ were conducted at atmospheric pressure in a fixed-bed continuous flow reactor consisting of a quartz tube with an inner diameter of 6 mm and a length of 300 mm. The tube was placed in a vertical tube furnace. The amount of the catalyst used during the catalytic runs was 0.05 g. The catalyst sample with particle diameter in the range from 0.20 to 0.25 mm was diluted with quartz (0.2–0.3 mm) and was packed in the reaction tube. In addition, a spent Ni catalyst with Ni/Si ratio of 0.3 was re-oxidized at 873 K in air for 1 h. Prior to each catalytic measurement the catalyst was reduced *in situ* by heating the catalyst in a flow of 10% H₂/N₂ (total flow rate 50 ml/min) from room temperature to 773 K at a rate of 10 K/min and maintaining this temperature for 1 h. The catalyst was purged with flowing nitrogen (60 ml/min) for 40 min to remove adsorbed hydrogen from the surface. A reactant gas mixture of CH₄ and CO₂ diluted with 60 ml/min N₂ has been used for CO₂ reforming of methane. The total flow rate was always kept at 100 ml/min. The reaction was conducted at temperatures of 773–873 K and CH₄/CO₂ ratios of 0.5–2. The reaction products were analyzed in a gas chromatograph (Varian 3700) equipped with a 3 m active carbon column (Carlo Erba) and a TCD.

3. Results

3.1. Catalysts characterization

3.1.1. Textural properties

The representative adsorption–desorption isotherms of the calcined MCM-41-supported Ni and PdNi samples are shown in Fig. 1. According to the IUPAC classification all samples show a type IV isotherm, which are characteristic of mesoporous materials [28]. At low relative pressure, formation of a monolayer of adsorbed molecules is the prevailing process. At high relative pressures, the adsorption in mesopores leads to multilayer formation and then condensation takes place, giving rise to a sharp adsorption volume increase. The shape of the isotherms becomes less inclined with increasing the Ni content. The isotherms of the samples have hysteresis loops that according to IUPAC are of H1 type, typical for mesoporous materials [29,30].

The textural characteristics of calcined samples are summarized in Table 1. All supported samples show lower values of the textural characteristics compared to those related to the MCM-41 support. The 0.3Ni sample has the highest specific surface area. The surface area, pore volume and pore diameter for bimetallic MCM-41-supported PdNi catalysts decrease with the increase of Ni content, which might be caused by blocking the pores with nickel oxide particles. The addition of Pd to 0.3Ni provokes a decrease of the values of S_{BET} and pore volume (Table 1). Probably, this is due to a partial redistribution of the nickel oxide particles after second step of impregnation with Pd precursor, thus blocking the pores [31].

Pore size distribution obtained from the desorption branch of the N₂ isotherm by the Barret–Joyner–Halenda method is shown in Fig. 2. The pore size distribution for 0.3Ni sample is quite narrow in the range 1.5–3 nm centred at 2.46 nm (Table 1). The pore size distribution for PdNi samples is approximately the same, but the peak is broader and centred at lower pore size values (2.1–2.3 nm).

3.1.2. XRD

XRD patterns of the calcined MCM-41 and PdNi/MCM-41 samples are shown in Fig. 3. Low-angle XRD patterns of the

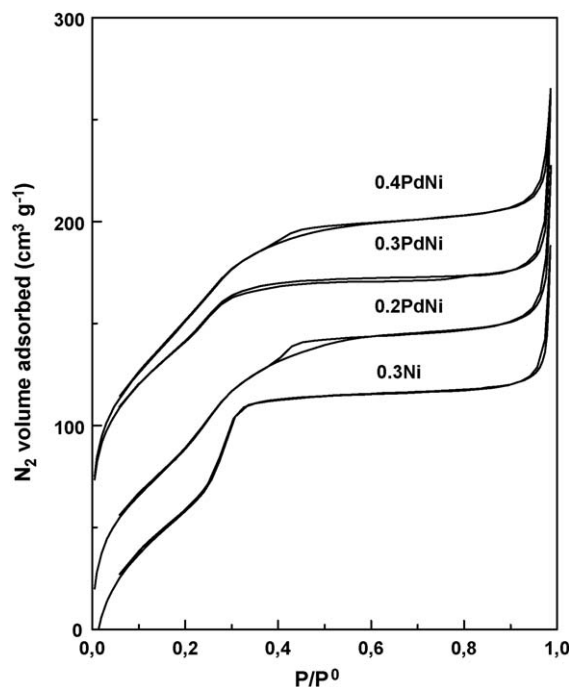


Fig. 1. Adsorption–desorption isotherms at 77 K of MCM-41-supported Ni and PdNi samples.

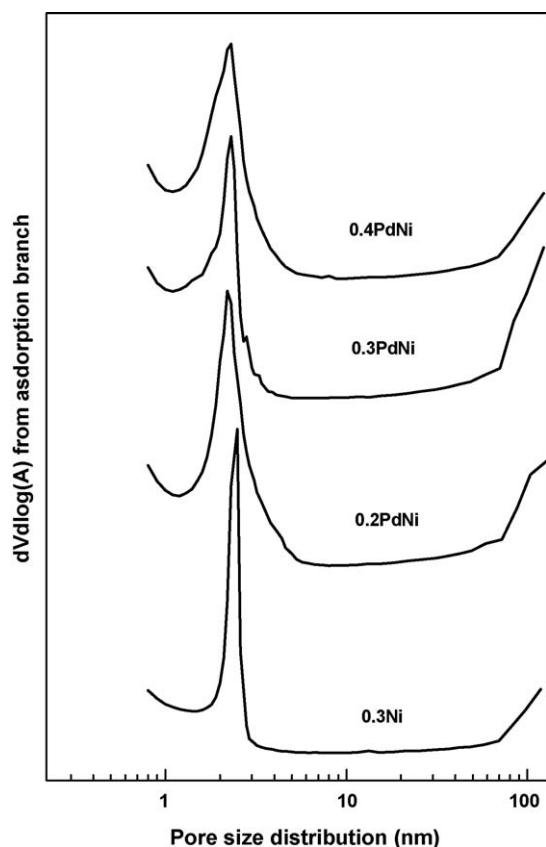


Fig. 2. BJH pore size distribution (desorption data) of MCM-41-supported Ni and PdNi samples.

samples (Fig. 3a) show Bragg peaks which are characteristic for MCM-41 structure. MCM-41 gives Bragg peak at the 2θ value of 2.42° , which corresponds to $d_{(1\ 0\ 0)}$ and two reflections at 4.14° and 4.80° . The position of Bragg peak changes slightly, depending on Ni concentration. A slight distortion of the MCM-41 structure is observed with increasing the Ni content. The values of 2θ of the main peak of the samples are 2.34° , 2.40° and 2.44° corresponding to Ni/Si ratios of 0.2, 0.3 and 0.4, respectively. Samples with Ni/Si ratio of 0.2 and 0.3 give two reflections. The sample with the highest Ni/Si ratio of 0.4 gives only one reflection may be, due to a distortion of MCM-41 structure caused by the increase of Ni content. The same tendency in the change of the position of Bragg peak was observed for MCM-41-supported monometallic Ni partners with the same Ni/Si ratios [22].

A NiO phase with characteristic diffraction peaks at $2\theta = 37.2^\circ$, 43.5° , 62.9° , 75.4° and 79.6° [21] is observed for all samples (Fig. 3b). There is no linear correlation between the amount of Ni and the intensity of NiO peaks. The XRD analysis shows that the highest NiO peak intensity is observed for PdNi with the highest Ni/Si ratio (0.4), followed by non-promoted with Pd Ni sample. A small peak at $2\theta = 33.9^\circ$ is also observed in the XRD profiles of bimetallic PdNi catalysts, belonging to PdO formation [32] (ICSD no. 24692).

A measurement of the NiO and PdO crystallite size, based on the peak width at half maximum [25], was carried out using the characteristic peaks at 43.5° and 33.9° , respectively. The NiO and PdO crystallite size values for the samples are listed in Table 1. It can be concluded that the presence of Pd in Ni-containing samples leads to a decrease of the NiO size. The 0.3PdNi sample reveals twice smaller NiO crystallites (12.3 nm) compared to that of its partner without Pd (25.7 nm). In addition, the bimetallic PdNi catalyst with Ni/Si ratio of 0.3 possesses smaller nano-sized NiO particles than the samples with ratios of 0.2 and 0.4 (13.9 and

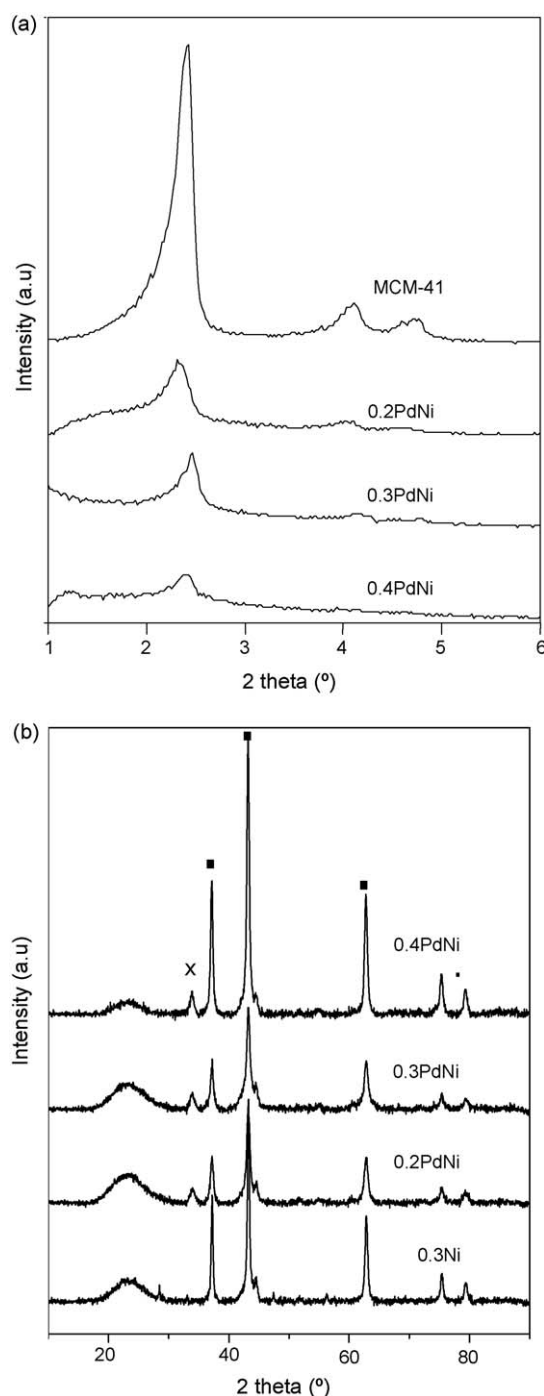


Fig. 3. XRD of MCM-41 and calcined supported Ni and PdNi samples: low-angle XRD in the range of $1\text{--}6^\circ$ (a) and XRD in the range of $10\text{--}90^\circ$ (■ NiO; × PdO) (b).

20.5 nm for 0.2PdNi and 0.4PdNi, respectively). It suggests that the addition of Pd leads to the formation of smaller nickel oxide species and therefore, to a higher dispersion of the nickel particles on the surface of PdNi sample with Ni/Si ratio of 0.3. The dimension of PdO crystallites for PdNi/MCM-41 samples with different Ni/Si ratios ranged between 5.8 and 6.8 nm (Table 1).

3.1.3. TPR

Temperature-programmed reduction experiments were performed to evaluate the reducibility of supported Ni and PdNi catalysts. Fig. 4 shows the TPR profiles of calcined supported bimetallic system. To facilitate the description of the TPR profiles of

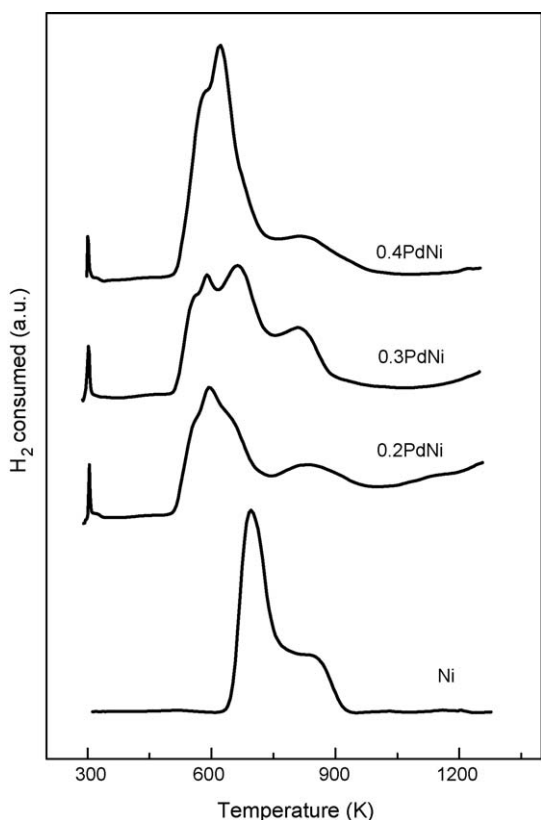


Fig. 4. TPR profiles of MCM-41-supported Ni and PdNi samples.

the samples, the TPR patterns are divided in three temperature regions: region I (295–312 K), region II (504–724 K) and region III (767–961 K). The region I is related to the reduction of PdO species. The smallest well defined TPR peak at 302 K observed for all samples is caused by the reduction of small PdO_x clusters [33] preferentially deposited on the surface of nickel oxides, as it was confirmed by XPS. In addition, the formation of such Pd oxide species is likely, considering the fact that the PdNi samples are prepared by impregnation of Pd onto Ni/MCM-41. This can be expected considering that palladium has a lower surface tension and a large atomic radius than Ni as well as the Ni is in a large excess compared to Pd. As a consequence, Pd tends to be expelled out of the Ni matrix leading to some Pd agglomeration [34]. For all PdNi samples the maximum in intensity of the PdO peak appeared at almost the same temperature that is an indication for similar particle size of palladium oxide species, confirmed by XRD (Table 1).

The regions II and III should be related to the reduction of supported Ni oxide species in different interaction with the carrier surface. It is well known that the interaction between the nickel oxide and the support can affect the reduction temperature. In the case of weak interaction, the nickel species can be easily reduced at lower temperature than in the case of a strong interaction. The intensity and the position of the peaks in regions II and III depend

on the Ni content of the samples. A broad peak with maxima at about 556, 596 and 663 K appears in the region II of the TPR profile of PdNi sample with the lowest Ni/Si ratio (0.2). This means a heterogeneous distribution of nickel oxide species interacting weakly with the support [34]. The TPR profile of 0.3PdNi, practically, has a similar shape of the TPR profile for 0.2PdNi sample since they show signals in common that is not evident for 0.4PdNi (Fig. 4). It should be noted that the hydrogen uptake for the peak at 663 K for the 0.3PdNi sample is larger compared to that for the sample with lower Ni/Si ratio (0.2). We would assume that this peak is originated from the reduction of NiO species in moderate interaction with the support. The heterogeneous distribution of NiO species observed for 0.4PdNi sample is revealed by the strong TPR peak at 622 K accompanied by a shoulder on the left side at 590 K (Fig. 4). However, the hydrogen consumption as well as the main peak maximum for 0.4PdNi sample is shifted by 38 K to lower temperature value compared to that for 0.3PdNi sample that could be related to different morphologies of nickel particles. A part of Ni species on 0.4PdNi is reduced at almost the same temperature as that on 0.2PdNi and 0.3PdNi samples. It is expected that the reduction of small NiO particles bound to the support surface, would be more difficult than the reduction of large particles where the interaction between NiO species and the support surface is rather weak. Therefore, the TPR results suggest that 0.4PdNi catalyst consists of a fraction of NiO particles of large mean diameter than 0.3PdNi catalyst. The latter is in agreement with the results of XRD (Table 1).

The hydrogen consumption peak in region III for all samples would be assigned to the reduction of highly dispersed Ni²⁺ species interacting strongly with the support and forming monolayer(s) of the nickel silicate at the surface region of MCM-41 substrate [35–37].

The TPR profile of the Pd-free Ni sample shows a strong peak at 695 K and a small one at 846 K (Fig. 4). It means that two kinds of nickel oxide species are formed; agglomerated NiO particles and well dispersed species in a strong interaction with the support. Addition of a small amount of Pd to MCM-41-supported Ni sample leads to start the reduction peak in region II at about 60 K lower than that for Pd-free Ni sample. This is clear evidence that the reduction of NiO is promoted by the presence of the noble metal. Palladium oxide precursor, which is reduced first to Pd⁰, is able to activate the hydrogen, thus favouring the reduction of nickel oxide species by spill-over [38]. This observation is similar to that observed previously in our report [21] where the addition of small amount of Pt to zeolite-supported Ni catalyst led to a shift of the TPR peak to lower value by 70 K. The evident temperature shift in the TPR profiles of PdNi samples compared to that of Pd-free Ni sample is considered to be due to the different nickel species on the monometallic and bimetallic catalysts. The TPR results suggest that the nickel oxide species interact with the support surface to different extent, depending on the Ni content and the presence of Pd.

3.1.4. XPS

The binding energies (BE) of Si 2p, O 1s, Ni 2p_{3/2} and Pd 3d_{5/2} core electrons as well as the values of the XPS atomic Ni/Si and Pd/Si ratios for reduced samples are summarized in Table 2. The BEs

Table 2

Binding energies (eV) of core electrons and XPS atomic ratios of H₂-reduced Ni and PdNi catalysts.

Sample	Si 2p	Ni 2p _{3/2}	Pd 3d _{5/2}	O 1s	Ni/Si	Pd/Si	Pd/Ni
0.3Ni	103.4	852.3 (20) ^a 855.6 (80) ^b	–	532.7	0.08	–	–
0.2PdNi	103.4	852.3 (23) 855.5 (77)	335.0	532.7	0.16	0.026	0.17
0.3PdNi	103.4	852.2 (46) 855.5 (54)	334.9	532.8	0.19	0.023	0.12
0.4PdNi	103.4	852.1 (46) 855.5 (54)	335.0	532.7	0.34	0.018	0.05

^a The percentages of Ni⁰.

^b The percentages of Ni²⁺.

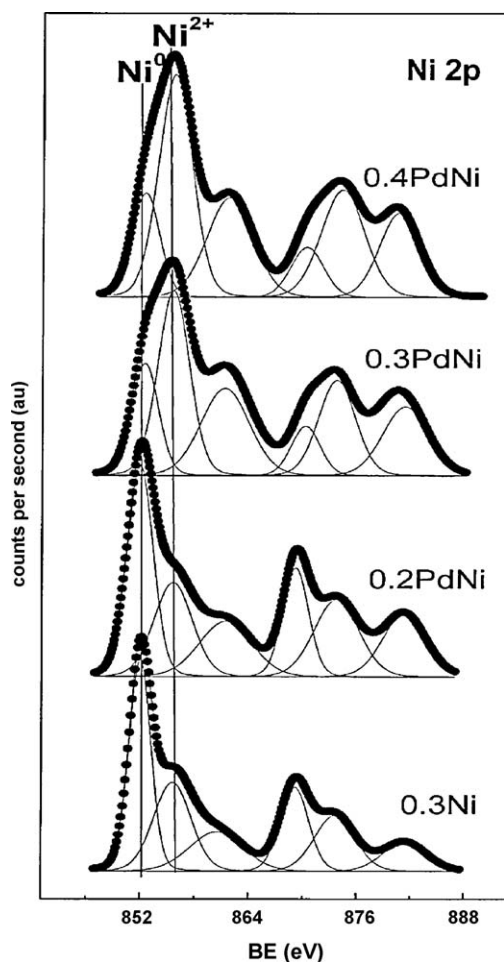


Fig. 5. XPS profiles of Ni 2p for reduced MCM-41-supported Ni and PdNi catalysts.

values of Si 2p and O 1s levels are 103.4 and 532.7 eV, respectively. The BE value of Pd 3d_{5/2} levels at 335.0 eV (Table 2) is an indication for the presence of Pd⁰ supported on silicon oxide [39]. The Pd-containing samples did not show any BE shift for Pd 4d_{5/2} core-level that suggests the absence of metal–support interaction, i.e. the electron transfer between the noble metal and the support or nickel can be excluded. The XPS spectra of Ni 2p core-levels for reduced Ni and PdNi samples are shown in Fig. 5. The Ni 2p_{3/2} spectral region for all reduced samples shows peak at ca. 852.1–852.3 eV, which is characteristic of Ni⁰ [40,41]. The observation of the satellite line is a proof of the presence of Ni²⁺ ions placed in an environment of oxide ions [42,43]. This finding, together with the appearance of the second component of Ni 2p_{3/2} at ca. 855.5 eV, which is related to the non-reduced nickel ions interacting with support lattice oxygen [38], is an indication that the nickel oxide particles are not completely reduced. The latter can be connected with the presence of some traces of nickel silicates (not detected by XRD) as well as of agglomerates.

The surface atomic ratios, calculated from the intensities of the peak normalized by atomic sensitivity factors [44], are summarized in Table 2. The XPS Ni/Si ratio for 0.3PdNi is approximately two times higher compared to that of its Pd-free partner, which is an indication for high dispersion of Ni particles. The addition of Pd to MCM-41-supported 0.3Ni catalyst leads to an increase of the amount of reduced nickel (from 0.20 to 0.46 for 0.3Ni and 0.3PdNi, respectively, Table 2). XPS results show that the reducibility of supported nickel oxide species depends on the Ni content (Table 2). The amount of reduced Ni increases with the increase of Ni/Si ratio from 0.2 to 0.3. Further increase of the nickel content (at Ni/

Si = 0.4) does not affect the reducibility of NiO particles, probably due to the presence of the biggest NiO particles, observed by XRD (Table 1). The fraction of reduced Ni for 0.3PdNi and 0.4PdNi sample is almost the same (about 46%, Table 2).

It should be noted that the XPS Ni/Si atomic ratio rises with the increase of Ni content in bimetallic PdNi catalysts (Table 2). However, the increase of XPS Ni/Si atomic ratio for 0.3PdNi compared to that for 0.2PdNi is twice lower than the difference observed for 0.3PdNi and 0.4PdNi in spite of the uniform rise of the Ni amount in the samples. The latter would be connected with the different morphology of the nickel particles. The thicker size of the nickel oxide layer (Table 1) over 0.4PdNi catalyst could be the reason for the increased XPS Ni/Si ratio (Table 2).

As opposite to the observation for the change of XPS Ni/Si atomic ratios, the XPS Pd/Si ratio decreases with the increase of Ni content (Table 2) that is surprising for samples with approximately the same Pd loading. The higher XPS Pd/Si surface ratios at lower Ni content (Ni/Si = 0.2 and 0.3) suggest that Pd is well dispersed on the catalyst surface; the palladium atoms are preferentially located on the nickel species, being confirmed by the higher value of the XPS Pd/Ni ratio relative to those of the XPS Pd/Si (Table 2). This is similar to the observations by other authors. The analysis of reduced bimetallic supported AuNi system by EXAFS [45] has shown that Au preferentially migrated to the surface of the nickel clusters under reduction, whereas when Ni is in an oxidized state the individual Au atoms interact only with other Au atoms and not with NiO.

3.1.5. HRTEM

The morphology of supported metal particles was examined by HRTEM. Particle size distribution was determined from TEM analysis of reduced and spent MCM-41-supported monometallic 0.3Ni and bimetallic 0.3PdNi catalysts (Fig. 6). It can be concluded, that irrespectively of the Pd-promotion, both freshly reduced and spent catalysts show a heterogeneous distribution of the metal particles (Fig. 6). There is a broad range of particle size up to near 80 nm for the reduced 0.3Ni sample (Fig. 6). In contrast, the particle size distribution is much narrower for reduced 0.3PdNi sample, with largest particle smaller than 35 nm. These results are in agreement with the average particle size of the oxide precursor NiO estimated from the XRD of calcined samples. The HRTEM average size of the metal particles for freshly reduced MCM-41-supported 0.3Ni and 0.3PdNi samples are of about 17.5 and 7.5 nm, respectively. The amount of large metal particles (above 30 nm) for reduced PdNi sample almost disappears after addition of noble metal (Fig. 6). At the same time, the amount of smaller particles in the range of 0–10 nm increases when Pd is present in the catalyst. It can be assumed that the addition of Pd to 0.3Ni/MCM-41 catalyst leads to formation of smaller nano-sized nickel particles, which results in a higher dispersion of metallic Ni phase. Such improvement of the nickel dispersion after modification of Ni/SiO₂ with Sr has been observed by Jing et al. [46].

For the spent Pd-free 0.3Ni catalyst, the average particle size increases approximately by 30% compared to that for freshly reduced sample (from 17.5 to 24.0 nm, Fig. 6). It means that an agglomeration of the particles occurs for the Pd-free Ni catalyst. The average particle size of bimetallic 0.3PdNi catalyst slightly changes after catalytic reaction. This indicates that Pd-promotion of Ni/MCM-41 catalyst prevents the strong sintering of metal particles during on-stream reaction.

3.2. CO₂ reforming of CH₄ and carbon formation

3.2.1. Catalytic behaviour of PdNi catalysts

The conversions of CH₄ and CO₂ as well as the yields of H₂ and CO are the generally accepted criteria for accessing the catalytic properties of the catalysts in the reaction of reforming of methane

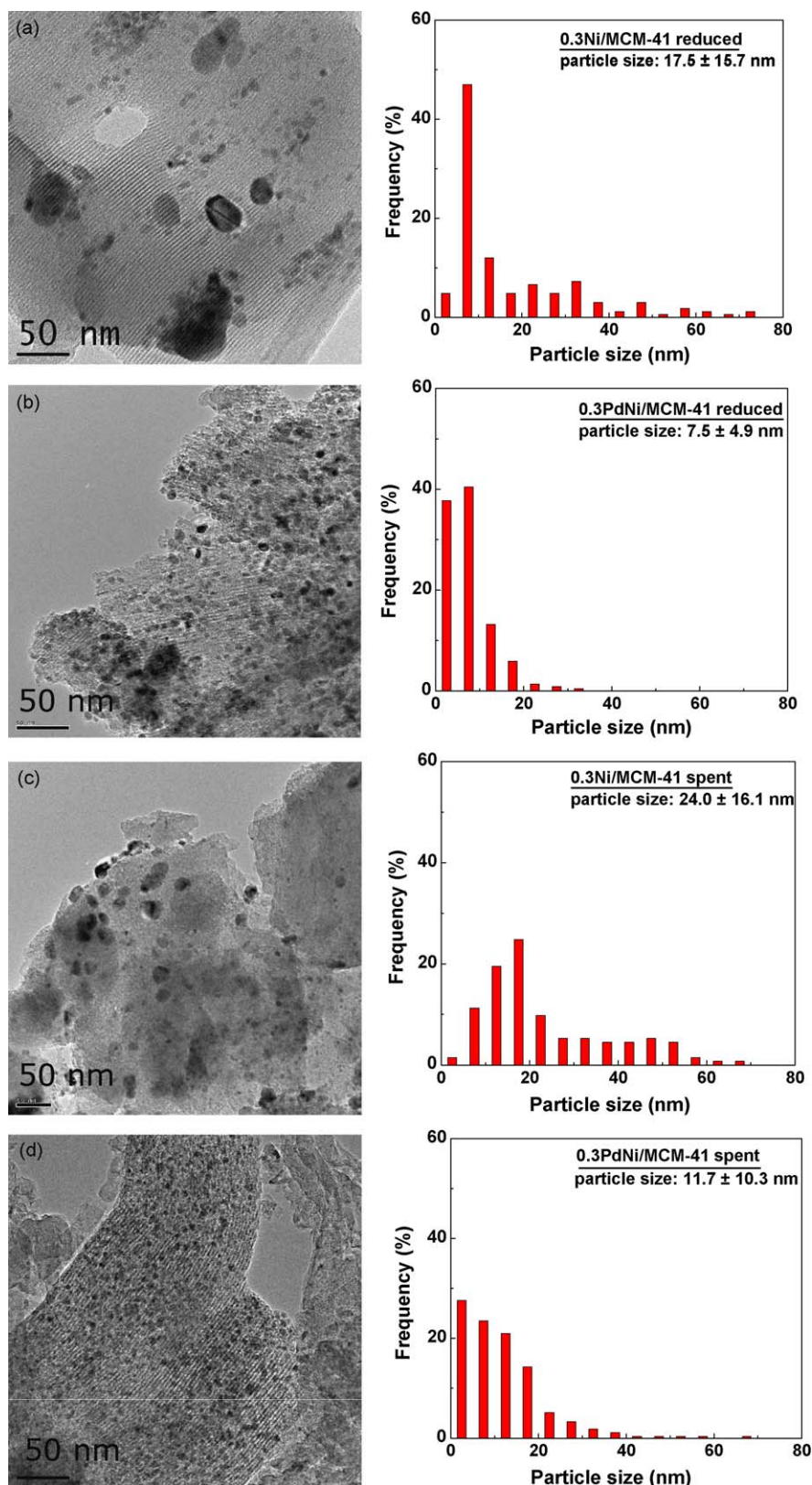


Fig. 6. Particle size distribution for reduced (a and b) and spent (c and d) MCM-41-supported Ni and 0.3PdNi catalysts determined from TEM.

with CO₂ (Eq. (1))



The effect of reaction temperature on the catalytic behaviours of PdNi sample with Ni/Si = 0.3 is depicted in Fig. 7. The CH₄ and

CO₂ conversions as well as the CO and H₂ yields increase with the increase of the reaction temperature.

The results of catalytic behaviours of MCM-41-supported Ni and bimetallic PdNi catalysts at reaction temperature of 823 K and at ratio of CH₄/CO₂ = 1 are summarized in Table 3. The results are determined at steady-state activity for all catalysts (120 min

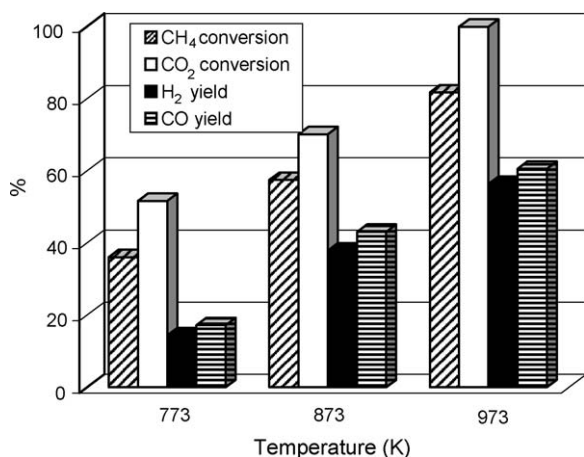


Fig. 7. Catalytic properties of MCM-41-supported 0.3PdNi catalyst as a function of reaction temperature at CH_4/CO_2 ratio of 1.

Table 3

Catalytic properties of MCM-41-supported Ni and PdNi catalysts in the reaction of dry reforming of methane at 120 min ($T_R = 823$ K; $\text{CH}_4/\text{CO}_2 = 1$).

Catalysts	CH_4 conversion (%)	CO_2 conversion (%)	H_2 yield (%)	CO yield (%)	H_2/CO
0.3Ni	16.2	24.5	10.7	14.8	0.69
0.2PdNi	22.8	30.8	14.4	17.3	0.83
0.3PdNi	36.1	51.7	19.8	24.5	0.81
0.4PdNi	30.0	41.6	17.5	21.7	0.81

on-stream). It should be mentioned that the values of CO_2 conversion are higher than those of methane conversion due to the occurrence of simultaneous reverse water gas-shift (RWGS) reaction (Eq. (2)) [47]. In addition, the H_2/CO ratios are less than 1 indicating the contribution of the RWGS reaction:



Addition of Pd to monometallic Ni catalyst (at $\text{Ni}/\text{Si} = 0.3$) leads to an increase of the conversions of CH_4 and CO_2 as well as of the H_2 and CO yields (Table 3). The activity of bimetallic PdNi catalysts is a function of the nickel content. There is an optimum loading beyond which the increase in nickel amount produces further decrease of the activity parameters. Maximum conversion of CH_4 and CO_2 as well as H_2 and CO yields are obtained for 0.3PdNi catalyst.

An apparent deactivation for bimetallic PdNi catalysts is not observed in Fig. 8. However, there is a significant difference between the catalytic performances of monometallic Ni and bimetallic PdNi catalysts. The activity of MCM-41-supported Ni catalyst decreases strongly with time (Fig. 8) the first 120 min and then it decreases slowly with time on stream. The initial catalyst deactivation of non-promoted 0.3Ni sample may be due to a combination of the nickel sintering in the presence of steam caused by RWGS as well as of the fast carbon deposition. From Fig. 8 it is observed that after re-oxidation of the spent 0.3Ni catalyst the change of catalytic behaviour follows the same tendency like initial catalyst, but the values are slightly lower compared to those of the non-oxidized catalyst. In addition, the initial activity of the regenerated 0.3Ni catalyst is not too high that would be related to the presence of some encapsulated carbon species difficult to be oxidized.

However, the addition of Pd to 0.3Ni catalyst changes drastically the catalytic behaviour of bimetallic system: the CH_4 and CO_2 conversions remain nearly constant. The same trend is observed for H_2 and CO yields over supported PdNi catalysts (Fig. 8c and d).

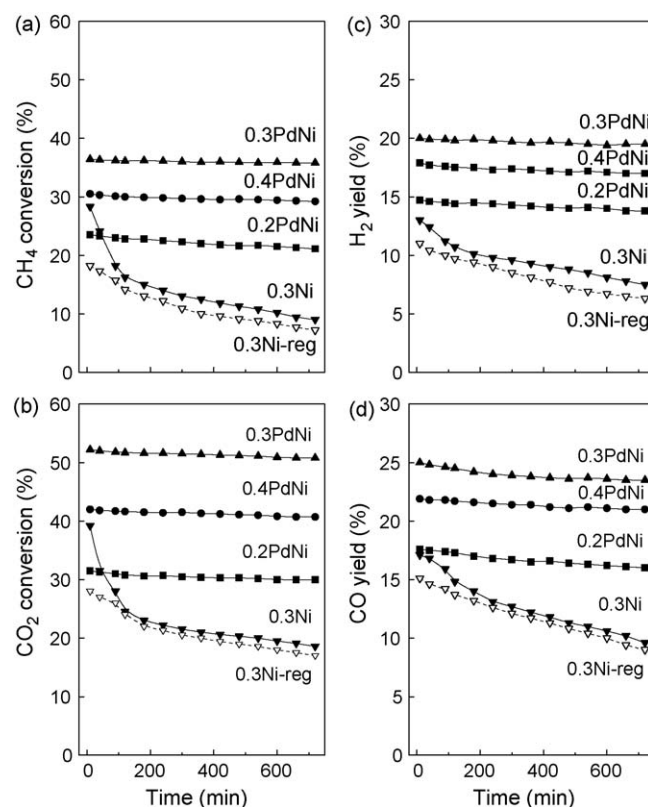


Fig. 8. Evolution of catalytic properties of MCM-41-supported Ni, PdNi catalysts and re-oxidized spent 0.3Ni sample (— — —) with time-on-stream at reaction temperature of 823 K and CH_4/CO_2 ratio of 1.

3.2.2. Carbon formation

The thermogravimetric (TG) and differential thermogravimetric (DTG) profiles of the temperature-programmed oxidation (TPO) in air of the spent catalysts are shown in Fig. 9. It should be noted that the contribution of the metal oxidation is negligible during temperature-programmed oxidation of the spent catalysts. Therefore, the weight loss revealed by the TG curves of the samples is mainly due to the removal of deposited carbon on the active metallic sites. The percentage of the weight loss of the samples increases in the following order: 0.3PdNi < 0.2NiPd < 0.3Ni < 0.4PdNi. The addition of Pd to monometallic 0.3Ni catalyst favours a decrease of the coke formation since the percentage of the weight loss for 0.3PdNi (65.3%) is lower than that observed for 0.3Ni sample (71.5%). Within the bimetallic system it is clear that the largest weight loss takes place for catalyst with the highest Ni content (78.8% for 0.4PdNi), where as the lowering the nickel content results in a less carbon formation. These observations seem to be conflicting with the results of stability of these catalysts, as shown in Fig. 8. However, the stability of the catalysts depends on several factors such as type of carbon deposit, coking rate, metal sintering, etc. This will be discussed in Section 4.

The DTG curves (Fig. 9) of the spent catalysts show a broad peak in the temperature region of 750–860 K with well defined shoulder. There is a change in the position and relative intensity of the peaks for all samples as a function of Ni content. This means different reactivity of carbon species toward oxidation to CO_2 . The reactivity of deposited carbon with oxygen in 0.3PdNi sample differs from the other spent catalysts. There is a displacement of the main peak position for 0.3PdNi sample to lower value (to 824 K) compared to those for 0.3Ni (847 K) and PdNi samples with Ni/Si ratio of 0.2 (843 K) and 0.4 (849 K). Typically, the lower temperatures are ascribed to coke which burns easier due to lower molecular weight and low density of deposited carbon structures.

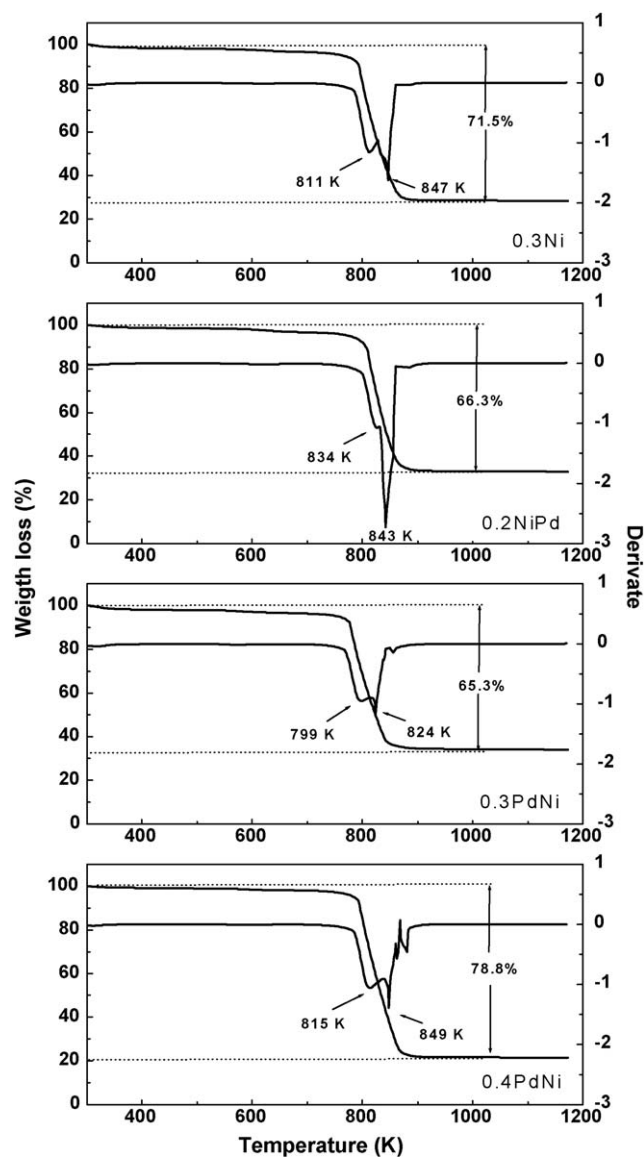


Fig. 9. TG and DTG profiles of spent MCM-41-supported Ni and PdNi catalysts.

It can be concluded that the less resistant carbon deposit toward oxidation dominates on the surface of 0.3PdNi catalyst. It should be noted that no measurable amounts of CO and water were observed during all the TPO experiments performed. The absence of water

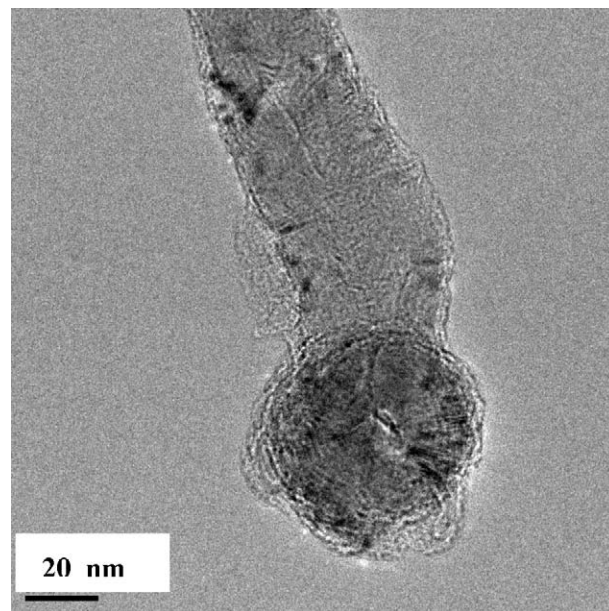


Fig. 11. TEM image of filamentous carbon.

strongly suggests that the carbonaceous species formed do not contain hydrogen. In addition, practically, there is no difference in the change of temperature oxidation and the amount of carbon for monometallic 0.3Ni and bimetallic 0.3PdNi catalyst with the highest Ni content. Further, TEM analysis of spent catalysts reveals clearly the formation of filamentous carbon over spent Ni and 0.3PdNi catalysts (Figs. 10 and 11).

4. Discussion

4.1. Catalyst materials

The activity of MCM-41-supported catalysts in terms of CH_4 conversion has the following order: 0.3PdNi > 0.4PdNi > 0.2PdNi > Ni. Comparing the S_{BET} of bimetallic PdNi catalysts with different Ni content (Table 1), the 0.2PdNi catalyst exhibiting the highest surface area is less active in dry methane reforming reaction compared to other catalysts (Table 3). A reversed trend is observed for PdNi samples with higher Ni content ($\text{Ni/Si} > 0.2$) which display lower surface area and higher catalytic activity within the bimetallic system. Monometallic Ni catalyst has the highest BET surface area, but it deactivates very fast. It is well known that the catalysts with high BET surface area can provide large contact area

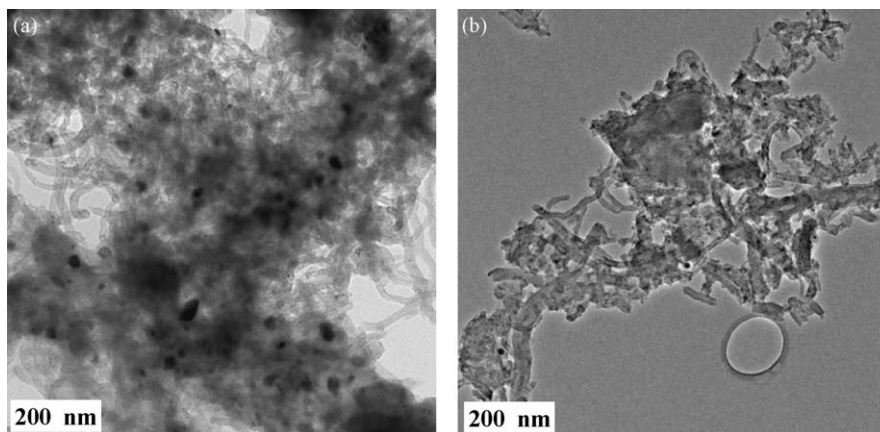


Fig. 10. TEM images of spent MCM-41-supported Ni (a) and PdNi (b) catalysts.

for the reactants, thus resulting in high activity. However, the fresh catalysts calcined at 823 K do not display measurable activity until they are reduced in H_2 -containing gas. In other words, the active sites on the catalysts must be metallic Ni and Pd that have been formed during hydrogen pre-treatment and/or during reaction. Therefore, catalyst activity should depend more on other factors, such as metal density, metal crystalline structure and metal-support environment, rather than the specific surface area.

Addition of Pd changes the reduction profile of nickel catalyst, favouring the reduction at lower temperatures. This occurs because palladium is reduced at a lower temperature than nickel and, once reduced, it is a H_2 dissociation site, and dissociated atomic hydrogen is a stronger reducing agent than molecular gaseous hydrogen [48]. The TPR profiles of the bimetallic PdNi system (Fig. 4) indicate that the Ni and Pd metals are formed from similar oxide precursor structure; nickel and palladium oxide species, respectively. The main reduction of Ni for bimetallic PdNi samples proceeds at lower wide temperature region compared to that for monometallic Ni sample, meaning that the metals are formed from the reduction of nickel oxides with different size. The XRD data showed the highest NiO precursor size for Pd-free catalyst (Table 1), which results in a more difficult reduction of agglomerated particles. A sintering of the active nickel metal phase occurs for the high metal content catalyst (0.4PdNi). The sintering leads to loss of both, the total and metallic surface area. The metal Ni dispersion for 0.4PdNi decreases having in mind the fraction of reduced nickel, which is similar to that observed for 0.3PdNi sample with lower Ni content, being confirmed by XPS data (Table 2). NiO species in interaction with the support with moderate strength prevail on the surface of 0.3PdNi catalyst. This leads to more easy reduction of nickel oxide species, which causes the increase of the fraction of reduced nickel. TPR and HRTEM results show heterogeneous distribution of metal particles on the surface of reduced and spent catalysts. The small difference in the XPS Ni/Si ratios of PdNi catalysts with Ni/Si ratios of 0.2 and 0.3 would be related to some decoration of a great portion of nickel surface with Pd species formed during preparation or pre-hydrogen treatment. This is confirmed by the higher values of XPS Pd/Ni ratios for these samples compared to that of bimetallic catalyst with the highest Ni loading (Ni/Si = 0.4, Table 2).

4.2. Activity and stability of catalysts

It should be noted that the number of the active sites is usually less than the total number of the surface metallic atoms [49]. Active sites could be crystalline defects and/or edges of metal particles. Better metal dispersion may lead to more active sites on the catalyst surface [49]. The particle size distribution in Fig. 6 indicates that the portion of the smaller particles is higher for bimetallic 0.3PdNi catalyst compared to that for monometallic Ni one. More small particles mean more edge and more active sites. In conclusion, even though 0.3PdNi catalyst has the lowest surface area among the investigated catalysts, the better metal dispersion and smaller metal particles give rise to more active sites that leads to the highest catalytic activity.

The increased activity of 0.3PdNi compared to that of 0.3Ni can be referred to the increase of the number of active metal sites present on the surface of bimetallic catalyst. An enrichment of the catalyst surface with small nickel particles in the presence of Pd occurs under reaction conditions that even takes place during reduction treatment of the 0.3PdNi sample (Fig. 6). In fact, XPS and TEM results clearly indicate the formation of small metal nickel particles. The high dispersion of Ni particles could also explain the relatively high stability of the bimetallic catalyst. It has been reported [19] that the high dispersion restrains the rate of carbon deposition, which increases the catalyst stability. However, a

significant amount of coke is deposited on the surface of the spent MCM-41-supported monometallic Ni and bimetallic PdNi catalysts as revealed by the TPO and HRTEM analyses. Most of the Ni particles and Pd species appear to be completely surrounded by carbon (Fig. 10).

However, metal particles over 0.3PdNi catalyst present almost the same average size as the ones of the freshly reduced sample (Fig. 6), which discards any significant sintering effect under reforming reaction. In addition, it is observed that some nickel particles are extracted from the MCM-41 support by growing carbon whiskers with metal particle placed on ends, as depicted in Fig. 11.

Catalyst deactivation and resistance to coking are two important issues of the reforming reaction of methane with carbon dioxide over nickel-based catalysts for their potential industrial applications. Two kinds of carbonaceous species, which exhibit different reactivity toward oxidation, are most often observed in CO_2 reforming of methane [50]: filamentous (whisker-like) carbon produced by adsorbed carbon atoms derived mainly from methane decomposition; and encapsulating hydrocarbon films (shell-like) formed by polymerization. The first kind of carbon species is characterized with lower temperature of oxidation to CO_2 compared to that of the second one.

Despite the large amount of carbon accumulated on the surface of bimetallic PdNi catalysts they show relatively high stability compared to that of monometallic Ni catalyst. The improved stability exhibited by bimetallic PdNi catalysts could be attributed to the more reactive form of carbon produced as compared to that formed over Ni catalyst. It is well known that the stability of the catalysts depends on several factors such as type of carbon deposit, coking rate and metal sintering. From qualitative point in view, coke deposits on Ni and Pd-doped Ni catalysts after 12 h of time on stream in dry reforming of methane at 823 K mostly consist of filamentous carbon, as was shown by TEM (Fig. 10). Such morphology is typical for supported Ni catalysts, in which nickel crystallites serve as catalysts for the growth of carbon filaments. As was discussed previously [51], the formation of filamentous carbon was associated with dissolution of carbon atoms (derived from CH_4 decomposition and CO dissociation) into the bulk of nickel crystallites, then diffuse through the metal followed by precipitation at the rear of the nickel particle to form a polymeric carbon filament. The kinetics of this process is influenced by the size and morphology of nickel particles, parameters that are different for the present catalysts, 0.3Ni and 0.3PdNi. Despite the analogous structure of carbon deposits it is evident that Pd inhibits the cooking process over Ni catalyst under reaction. TG data of the spent catalysts, shown in Fig. 9, quantitatively confirm the above evidence on the inhibition effect of palladium on the amount of carbon deposition over 0.3PdNi catalyst.

The formation of filamentous carbon on the surface of bimetallic PdNi catalysts has no negative effect on their activity and stability, being seen in Fig. 8. The bimetallic catalysts exhibit relatively good stability with time on stream, despite the significant amount of carbon deposition. This would be related to the site location of carbon. Great part of the metallic Ni particles could be located on the tip of filamentous carbon (Fig. 11) which catalyze CH_4 decomposition and hence determine the growth of the fibers [52]. The Ni metal particle at the tip of filamentous carbon has almost the same size as that of the diameter of the filament being seen from the Fig. 11. This is in agreement with earlier reports [52–54]. The edges of the stacking carbon layers are exposed at the walls of the fibers, and these layers adopt a turbostratic graphite structure as a consequence of the randomly displaced C-atoms with respect to each other [52,53]. Such a process can explain both the large amount of carbon formation on the catalyst surface and the catalyst stability with high activity

with time on stream. However, the reaction stops when methane and carbon dioxide do not have access to Ni particles in the presence of encapsulated amorphous carbon [14].

It was reported that the CH₄ decomposition on the metal surface, which is the initial step of reforming reaction, provides the major carbon species for carbon formation over catalyst [7]. Accordingly to Verykios and co-worker [55] the activation of CO₂ occurs on the support. At higher reaction temperatures, carbon is mainly produced from CH₄ decomposition, but when the temperature decreases the CO disproportionation becomes predominant. TEM analysis (Fig. 10) shows that the filamentous carbon is mainly formed on 0.3Ni and 0.3PdNi catalysts. In addition, a formation of encapsulated amorphous carbon on the catalyst surface cannot be excluded. For the spent Pd-free Ni sample traces of encapsulated carbon might be observed (Fig. 8) being supported by the lower initial activity after regeneration of the catalyst.

It has been demonstrated that the net formation of carbon on Ni-based catalysts is connected with the Ni particle size. Osaki et al. [56] related the carbon inhibition to the metal ensemble in catalysts and concluded that smaller ensembles are able to suppress carbon formation, as opposite to the large nickel clusters which are prone to carbon formation. In the literature different critical particle sizes have been reported: 7 nm [57] or 10 nm [49] for methane reforming with CO₂ below which carbon deposition can be avoided. The particle size for spent monometallic 0.3Ni catalyst is much higher compared to above-mentioned values (Fig. 6) and the amount of deposited carbon is also high. However, the addition of noble metals [21], Co [49], Ag [10], Sr [46] or sulphur passivation of nickel catalyst [58] leads to formation of smaller ensembles which suppress the carbon formation.

It is important to note, that the carbon formation occurs when the formation rate of carbon species is higher than its removal rate through reforming reaction [58]. On other hand, the relatively stable performance obtained for zeolite-supported bimetallic PtNi catalysts [21] has been explained by the equilibrium concentration of Pt–Ni particles and surface carbon species on Ni crystallites in spite of the carbon deposition. The stability of PtNi catalysts was connected with the existence of small Ni metal particles on the surface caused by the “dilution” effect of Pt [21]. The good coke resistance ability of noble metal promoted Ni catalysts was attributed to the formation of noble metal–Ni particles or clusters, which leads to an increase of Ni dispersion and favouring the formation of more reactive intermediate carbonaceous species.

It was reported [55] that the activation of CO₂ is a structure-sensitive reaction, i.e., the small particle size accelerates its activation. Comparing the metal particle size of 0.3Ni and 0.3PdNi catalysts it would be assumed that the small particle size for bimetallic catalyst could activate the CO₂ dissociation. In addition, the critical particle size to suppress the carbon formation over 0.3PdNi catalyst is ≤ 11.5 nm that is in accordance with the observations by other authors [49]. According to the conceptual model proposed by Zhang et al. [49], carbon formation and its removal depends on the metal particle size during dry CH₄ reforming: the small metal particles below 10 nm are crucial to the suppression of carbon. In the presence of large metal particles (≈ 20 nm), similar to our results for Ni sample, the carbon species formed near the periphery of the metal particles is easy to react with activated CO₂ to form CO [49]. However, when the carbon species far away from the periphery of metal particles tend to nucleate, the carbon deposits are accumulated on the large particles with time on stream that results in activity loss.

It should be noted that the initial catalyst activity has a direct correlation with the active metal content. A high metallic surface

leads to a high initial activity. Monometallic Ni catalyst has a high initial activity that decreases with time on stream. The formation of large particles and low metal dispersion for Ni catalyst under reaction conditions results in a rapid carbon formation and activity decay. The high carbon resistance of bimetallic 0.3PdNi catalyst might be attributed to its high metal dispersion and smaller metal ensembles. However, comparing the activity of monometallic and bimetallic catalysts shows that the synergy between Ni and Pd makes a significant difference. Similar to previously reports [21,49] the combination of noble metal and nickel significantly improved the catalyst activity for carbon dioxide reforming of methane as a result of the increased number of metal surface atoms. The metal dispersion is enhanced by the synergy Ni–Pd in the bimetallic catalyst with Ni/Si ratio of 0.3. The degree of reduction for 0.3PdNi catalyst is higher compared to that for monometallic Ni catalyst, as confirmed by the lower TPR peak and larger amount of Ni⁰ defined by XPS (Table 2).

The lower steady-state activity of monometallic 0.3Ni catalyst compared to that of bimetallic 0.3PdNi catalyst would be related mainly to the following reasons: (i) A large amount of carbon is accumulated on Ni catalyst that can reduce the available metal active surface area; and (ii) agglomeration of nickel particles takes place over non-promoted Ni catalyst. The metal surface of 0.3PdNi catalyst consists of a large fraction of nickel particles of smaller size than those of Ni catalyst. The amount of H₂ consumed in the higher temperature region of 550–850 K in the case of 0.3Ni catalyst is much higher compared to that of 0.3PdNi catalyst. It is expected that the reduction of small NiO particles, chemically bound on the support surface, would be more difficult than the reduction of large particles.

Addition of Pd to Ni-containing catalysts results in an enhancement of the conversions of CH₄ and CO₂ (Table 3). However, the activity and stability of the catalysts is not achieved by simply adding the noble metal. It seems that an optimal Ni/Si ratio is necessary for obtaining the best catalyst performance with respect to activity and stability. In our study the optimum level of Ni loading in PdNi/MCM-41 catalysts is observed at Ni/Si ratio of 0.3.

5. Conclusions

PdNi catalysts with different nickel content (Ni/Si of 0.3, 0.4 and 0.5) supported on mesoporous MCM-41 demonstrate good performance for carbon dioxide reforming of methane. Comparative studies conducted with supported monometallic 0.3Ni and bimetallic 0.3PdNi catalyst with the same nickel content show that the superior catalytic performance of Pd promoted Ni catalyst comes from the synergy effect between Ni and Pd in the bimetallic system providing good metal dispersion, high degree of reduction and high metallic surface area. However, within the bimetallic system, the catalytic performance of the catalysts depends on the nickel content. The Ni/Si ratio of 0.3 is optimal to achieve the highest activity of 0.3PdNi catalyst related to decrease of carbon deposition caused by the formation of smaller particles and higher metal dispersion compared to those of the sample with the highest Ni content (Ni/Si ratio of 0.4).

Acknowledgements

The financial support of the projects between the National Council of Scientific Research, Spain, and TUBITAK and Bulgarian Academy of Sciences is gratefully acknowledged. The authors acknowledge financial support by project no. X-1515/05 from National Science Fund at the Bulgarian Ministry of Education and Science. The authors gratefully acknowledge Dr. M.A. Peña (ICP-CSIC) for the DT/TGA measurements.

References

- [1] D.L. Trimm, *Catal. Rev.-Sci. Eng.* 16 (1977) 155.
- [2] J.R. Rostrup-Nielsen, *J. Catal.* 144 (1993) 38.
- [3] S.M. Gheno, S. Damyanova, B.A. Riguette, C.M.P. Marques, C.A.P. Leite, J.M.C. Bueno, *J. Mol. Catal. A: Chem.* 198 (2003) 263.
- [4] S. Damyanova, J.M.C. Bueno, *Appl. Catal. A: Gen.* 253 (2003) 135.
- [5] S. Duan, S. Senkan, *Ind. Eng. Chem. Res.* 44 (2005) 6381.
- [6] O. Yamazaki, T. Nozaki, K. Omata, K. Fujimoto, *Chem. Lett.* (1992) 1953.
- [7] J.R. Rostrup-Nielsen, J.H. Back Hansen, *J. Catal.* 144 (1993) 38.
- [8] Z.L. Zhang, X.E. Verykios, *Catal. Today* 21 (1994) 589.
- [9] J.S. Chang, S.E. Park, H. Chon, *Appl. Catal. A: Gen.* 145 (1996) 111.
- [10] N.V. Parizotto, K.O. Kocha, S. Damyanova, F.B. Passos, D. Zandut, C.M.P. Marques, J.M.C. Bueno, *Appl. Catal. A: Gen.* 330 (2007) 12.
- [11] J. Guo, H. Lou, X. Zheng, *Carbon* 45 (2007) 1314.
- [12] X.E. Verykios, *Int. J. Hydrogen Energy* 28 (2003) 1045.
- [13] B.S. Liu, C.T. Au, *Appl. Catal. A: Gen.* 244 (2003) 181.
- [14] X. Zhu, P. Huo, Y. Zhang, D. Cheng, C. Liu, *Appl. Catal. B: Environ.* 81 (2008) 132.
- [15] L. Pelletier, D.D.S. Liu, *Appl. Catal. A: Gen.* 317 (2007) 293.
- [16] J. Zhang, H. Wang, A.K. Dalai, *J. Catal.* 249 (2007) 300.
- [17] Z. Hou, P. Chen, H. Fang, X. Zheng, T. Yashima, *Int. J. Hydrogen Energy* 31 (2006) 555.
- [18] M. Nurunnabi, K. Fujimoto, K. Suzuki, B. Li, S. Kado, K. Kunimori, K. Tomishige, *Catal. Commun.* 7 (2006) 73.
- [19] C. Crisafulli, S. Scire, S. Minico, L. Solarino, *Appl. Catal. A: Gen.* 225 (2002) 1.
- [20] G.C. Araujo, S.M. Lima, J.M. Assaf, M.A. Peña, J.L.G. Fierro, M.C. Rangel, *Catal. Today* 133/135 (2008) 129.
- [21] B. Pawelec, S. Damyanova, K. Arishtirova, J.L.G. Fierro, L. Petrov, *Appl. Catal. A: Gen.* 323 (2007) 188.
- [22] C. Sener, K. Arishtirova, R.N. Nikolov, T. Dogu, G. Dogu, S. Damyanova, in: K. Hadjiivanov, V. Valtchev, S. Mintova, G. Vayssilov (Eds.), *Topics in Chemistry and Material Science: Advanced Micro- and Mesoporous Materials 1* (2008) 355.
- [23] Y. Park, T. Kang, J. Lee, P. Kim, H. Kim, J. Yi, *Catal. Today* 97 (2004) 195.
- [24] H. Wan, X. Li, S. Ji, B. Huang, K. Wang, C. Li, *J. Natural Gas Chem.* 16 (2007) 139.
- [25] H.P. Klug, L.E. Alexander, *X-ray Diffraction procedures for Polycrystalline and Amorphous Materials*, 2nd ed., Wiley-Interscience, New York, 1974.
- [26] D.A. Shirley, *Phys. Rev. B* 5 (1972) 4709.
- [27] P.M.A. Sherwood, in: D. Briggs, M.P. Seah (Eds.), *Practical Surface Analysis*, Wiley, New York, 1990, p. 181.
- [28] G. Leofanti, M. Padovan, G. Tozzola, B. Venturelli, *Catal. Today* 41 (1998) 207.
- [29] K. Kaneko, *J. Membr. Sci.* 96 (1994) 59.
- [30] S.G. Gregg, K.S.W. Sing, *Adsorption, Surface area and Porosity*, Academic Press, London, 1982.
- [31] V. Cáceres, J.L.G. Fierro, M.N. Blanco, H.J. Thomas, *Appl. Catal.* 10 (1984) 333.
- [32] E. Kanazaki, S. Tanaka, K. Murai, T. Moriga, J. Motonaka, M. Katoh, I. Nakabayashi, *Anal. Sci.* 20 (2004) 1069.
- [33] S. Subramanian, R.J. Kudla, C.R. Peters, M.S. Chattha, *Catal. Lett.* 16 (1992) 323.
- [34] V.L. Barrio, P.L. Arias, J.F. Cambra, M.B. Güemez, P. Pawelec, J.L.G. Fierro, *Appl. Catal. A: Gen.* 242 (2003) 17.
- [35] Z. Xu, Y. Li, J. Zhang, L. Chang, R. Zhou, Z. Duan, *Appl. Catal. A: Gen.* 210 (2001) 45.
- [36] J.-H. Lee, E.-G. Lee, O.-S. Joo, K.-d. Jung, *Appl. Catal. A: Gen.* 269 (2004) 1.
- [37] Z. Hou, O. Yokota, T. Tanaka, T. Yashima, *Appl. Catal. A: Gen.* 253 (2003) 381.
- [38] B. Li, S. Kado, Y. Mukainakano, M. Nurunnabi, T. Miyao, S. Naito, K. Kunimori, K. Tomishige, *Appl. Catal. A: Gen.* 304 (2006) 62.
- [39] B. Schleich, D. Schmeisser, W. Gopel, *Surf. Sci.* 191 (1987) 367.
- [40] Y.J. Huang, J.A. Schwarz, *Appl. Catal.* 36 (1988) 163.
- [41] P. Legare, A. Fritsch, *Surf. Interface Anal.* 15 (1990) 698.
- [42] B. Pawelec, R. Mariscal, R.M. Navarro, J.L.G. Fierro, *Microporous Mesoporous Mater.* 34 (2000) 181.
- [43] J.G. Kim, D.L. Pugmire, D. Battaglia, M.A. Langell, *Appl. Surf. Sci.* 165 (2000) 70.
- [44] C.D. Wagner, L.E. Davis, M.V. Zeller, J.A. Taylor, R.H. Raymond, L.H. Gale, *Surf. Interface Anal.* 3 (1981) 21.
- [45] Y.H. Chin, D.L. King, H.S. Roh, Y. Wang, S.M. Heald, *J. Catal.* 244 (2006) 153.
- [46] Q. Jing, H. Lou, J. Fei, Z. Hou, X. Zheng, *Int. J. Hydrogen Energy* 29 (2004) 1245.
- [47] J.S.B. Wang, S.Z. Hsiao, T.J. Huang, *Appl. Catal. A: Gen.* 246 (2003) 197.
- [48] J.A.C. Dias, J.M. Assaf, *Appl. Catal. A: Gen.* 334 (2008) 243.
- [49] J. Zhang, H. Wang, A. Dalai, *Appl. Catal. A: Gen.* 339 (2008) 121.
- [50] M.A. Goula, A.A. Lemonidou, A.M. Efstathiou, *J. Catal.* 161 (1996) 626.
- [51] S. Irueta, L.M. Cornaglia, E.A. Lombardo, *J. Catal.* 210 (2002) 263.
- [52] R.M. Navarro, M.A. Peña, J.L.G. Fierro, *Chem. Rev.* 107 (2007) 3952.
- [53] J. Ashok, S.N. Kumar, A. Venugopal, V.D. Kumari, M. Subrahmanyam, *J. Power Sources* 164 (2007) 809.
- [54] K. Otsuka, H. Ogihara, S. Takenaka, *Carbon* 41 (2003) 223.
- [55] V.A. Tsipouriari, X.E. Verykios, *Catal. Today* 64 (2001) 83.
- [56] T. Osaki, T. Mori, *J. Catal.* 204 (2001) 89.
- [57] J.-H. Kim, D.J. Suh, T.-J. Park, K.-L. Kim, *Appl. Catal.* 197 (2000) 191.
- [58] J.R. Rostrup-Nielsen, *J. Catal.* 85 (1984) 31.